Journal of Interfaces, Thin films, and Low dimensional systems 4 (1) Summer and Autumn (2020) 347-356

The influence of deposition rate on optical and microstructural characteristics of nanostructured ZnSe films prepared by thermal evaporation technique

Scientific research paper

Soodeh Momeni[1], Mohsen Ghasemi[1,2*], and Afrouz Taherian[3]

[1]*Department of Physics, Faculty of Sciences, Shahrekord University, Shahrekord, Iran*

[2]*Nanotechnology Research Institute, Shahrekord University, Shahrekord, Iran*

[3]*Faculty of Physics, University of Isfahan, Isfahan, Iran*

ARTICLE INFO

Article history:
Received 24 May 2021
Revised 18 August 2021
Accepted 28 August 2021
Available online 30 October 2021

Keywords:
Thermal evaporation technique
Nanostructured ZnSe films
Deposition rate
Optical properties
Microstructural properties

ABSTRACT

In this research, ZnSe thin films were deposited on glass substrate by the thermal evaporation method with deposition rates of 0.2, 0.4, 0.6, and 0.8 nm/s and with a constant thickness of 250 nm. All samples were annealed for 100 minutes at a temperature of 400 °C. Various techniques such as UV–Vis spectrophotometer, X-ray diffraction (XRD) analysis, and scanning electron microscope (SEM) were used to investigate different physical parameters such as energy band gap, refractive index, extinction coefficient, dielectric constant, and porosity of the ZnSe thin films. The influence of the deposition rate on the mentioned parameters was investigated. The XRD patterns showed that the ZnSe thin films have a cubic structure. The structural parameters such as lattice constant, crystallite size, strain, and dislocation density were determined for different samples. The maximum average transmittance of %93.1 in the visible wavelength region was obtained for the deposition rate of 0.6 (nm/s). The optical band gap was calculated using the derivation of absorption spectrum fitting (DASF) method, and the values of the energy band gap were obtained in the range of 3.71 ± 0.01 to 3.98 ± 0.01 eV. The XRD results acquired from the Williamson-Hall method showed that the crystallites size and strain of different samples were achieved in the range of 21.6 ± 1.1 to 42.9 ± 2.3 nm and $(0.61\pm0.02)\times10^{-3}$ to $(2.89\pm0.04)\times10^{-3}$, respectively. Finally, the relation between the optical and microstructural properties of the ZnSe films was studied.

1 Introduction

In recent years, thin-film science has grown considerably among various scientific domains as much research has been done in this field. Among optical thin films, semiconductors play an important role. ZnSe is a semiconductor of two known compounds with a bright yellow color that has two hexagonal and cubic crystalline structures [1]. This compound has high chemical stability, and it's interesting properties include a wide band gap, high refractive index, and high optical sensitivity [2–5]. Based on these special properties, ZnSe has various applications in thin film solar cells as buffer layer [6–8], cell imaging, humidity and gas sensors [9], thin film transistors [10], lasers [11], photo-detectors [12], blue-green zone of visible wavelength in light-emitting diodes [13], field emitter [9], and hydrophobic coating [14]. Therefore, the study of optical properties and detailed structural analysis are important to provide knowledge on the promising ZnSe material. Different methods have been used to

*Corresponding author.
Email address: Ghasemi.mohsen@sku.ac.ir, mphdghasemi@Gmail.com
DOI: 10.22051/jitl.2021.36255.1054

deposition of ZnSe thin films, such as RF magnetron sputtering [15], spray pyrolysis [16], chemical bath deposition [17], molecular beam epitaxy [18], and vacuum evaporation [19].

The ZnSe thin film prepared with the thermal evaporation technique are uniform and adherent. The optical and microstructural properties of ZnSe thin films have been investigated by some growth conditions such as substrate temperature, thickness, and post-deposition annealing temperature [20]. To the best of our knowledge, according to the literature, less attention has been paid to the effect of deposition rate on optical and microstructural properties of ZnSe thin films deposited by the thermal evaporation technique. In this research, the effect of deposition rate on the various parameters such as transmittance, reflectance, optical band gap, extinction coefficient, refractive index, real and imaginary dielectric constants, lattice constant, crystallite size, strain, and dislocation density of the ZnSe thin films, is investigated. Since the relationship between them is not yet fully understood and requires further research, in this work, an appropriate correlation is established between the various parameters, including the optical and microstructural properties of ZnSe thin films. We also attempt to express the interpretation for each of the phenomena that occurrs in different sections.

2 Experimental details

In this study, ZnSe thin films are deposited on the glass substrate. The cleanliness of the substrate surface is very important and affects the uniformity, optical and structural properties of the film. For cleaning of the substrate surface, the substrates were washed sequentially, in acetone, ethanol, isopropanol, Methanol, and then deionized water in an ultrasonic apparatus (Parsonic 2600s, Pars Nahand Engineering Company) for ten minutes. The substrates were placed in a vacuum chamber after drying with nitrogen gas flow. The thermal evaporation system (Yar Nikan Saleh Company, Iran) was used for film deposition. The vacuum chamber is depleted to the base pressure of $2\times10^{-5}\,mbar$. The ZnSe powder (Sigma Aldrich Company) was used as the target material with 99.99% purity. The thickness of the films and deposition rate were controlled using the quartz crystal system. Samples were prepared at ambient temperature and deposition rates of 0.2, 0.4, 0.6 and 0.8 nm/s and in the same thickness of 250 nm. All samples were annealed in a vacuum with the same conditions at 400 °C for 100 minutes after the growth process to improve the optical properties of ZnSe thin films. The image of the fabricated samples at different deposition rates, before and after the annealing process, is shown in Fig. 1. Transmittance data and optical reflection of the films were measured by a double-beam spectrophotometer (Shimadzu UV-3100 model). The microstructure of ZnSe films was determined using X-ray diffraction (XRD, X′ Pert-Pro MPD, Panalytical Company) and the surface morphology of ZnSe films was determined using Scanning Electron Microscope (SEM, VEGA-TESCAN-LMU model).

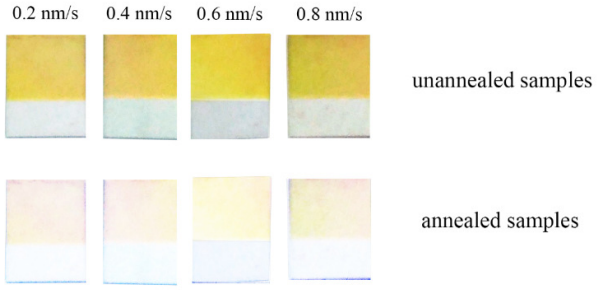

Figure 1. Image of the fabricated ZnSe thin films at different deposition rates, before and after the annealing process.

3 Discussion

The transmission (T) of ZnSe thin films was measured versus wavelength (λ) using a spectrophotometer apparatus. The transmittance of the samples, with various deposition rates before and after the annealing process, is shown in Figs. 2a and 2b, respectively. The presence of ripples in Fig. 2a can illustrate the interference effects inside the film. Thin film interference is a phenomenon in which light waves reflected from the upper and lower boundaries of a thin film interfere with each other, and their interference can be constructive or destructive. Following this phenomenon, maxima and minima occur in the transmission spectrum, and its diagram shows the oscillating behavior.

Figure 2b shows the transmittance spectrum of the films after annealing at 400 °C. According to this figure, by increasing the deposition rate, the absorption edge has been shifted towards a longer wavelength. This change in the transmittance spectrum can be

related to a change in the structural nature of the films [20]. The absorption edge is located in the ultraviolet region for all samples. As shown in Fig. 2b, transmission in the visible region is uniform due to heat treatment, and its value is more than %83 for all samples in this region. According to the figure, its average value in the visible wavelength region for the deposition rates of 0.2, 0.4, 0.6 and 0.8 nm/s, is %83.5, %90.5, %93.1 and %86.9, respectively.

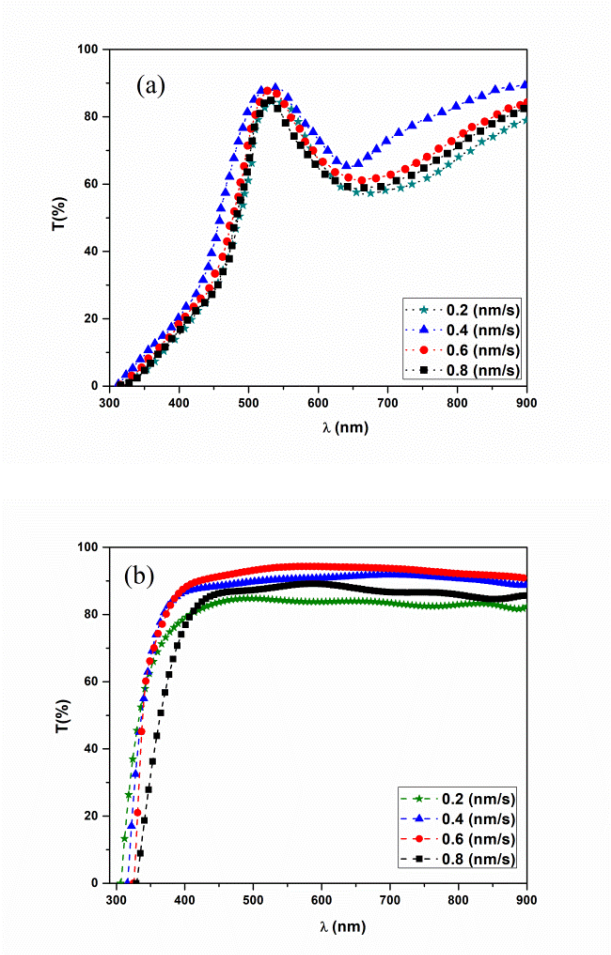

Figure 2. Plot of the transmission as a function of wavelength with different deposition rates (a) before annealing, (b) after annealing at 400 °C.

In general, the transparency of the films has improved after the annealing process. The reflection of the samples after the annealing process is shown in Fig. 3. As can be seen, the amount of the reflection in the visible region is less than %20, which is due to the dispersion and more transmission of these films in this region [21].

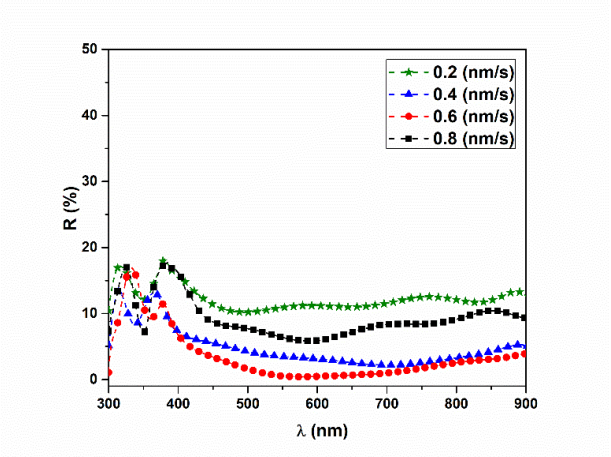

Figure 3. Plot of reflection of ZnSe thin films deposited at different deposition rates after annealing at 400 °C.

The absorption coefficient ($\alpha(\lambda)$) can be obtained from reflection and transmission data as follows [22]:

$$\alpha = \frac{1}{d}\ln\left(\frac{(1-R)^2}{T}\right), \quad (1)$$

Where α, d, R, and T are the absorption coefficient, film thickness, reflectance and transmittance, respectively.

To further investigate the optical properties of the samples, the extinction coefficient (k) and refractive index (n) were calculated. The extinction coefficient (k) is obtained as follows:

$$k = \frac{\alpha\lambda}{4\pi}. \quad (2)$$

In this equation λ is the photon wavelength. The extinction coefficient as a function of wavelength is shown in Fig. 4a. According to this plot, the extinction coefficient of the samples in the ultraviolet region is higher than its value in the visible region, which indicates that the films are transparent in the visible region. For all samples, the extinction coefficients are almost constant and uniform, which shows that the annealing of the samples are well done and the samples are more regularized after heating [23].

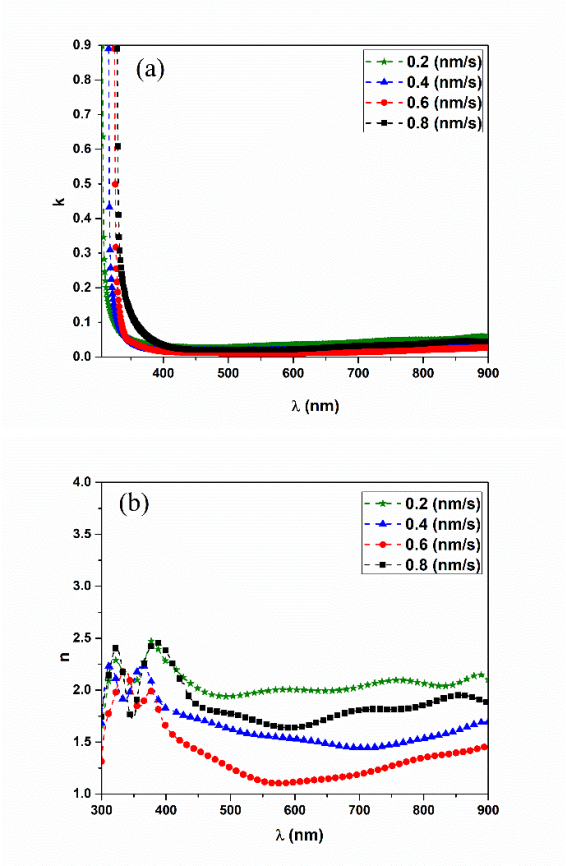

Figure 4. (a) Extinction coefficient, and (b) refractive index versus wavelength for the samples with different deposition rates, after annealing at 400 ℃.

The refractive index is one of the essential properties of an optical material because the refractive index is attributed to the electron polarization of the ions and the local field within the material [24]. The refractive index (n) was calculated using Eq. (3), which is written as a function of reflection (R) and extinction coefficient (k):

$$n = \left(\frac{1+R}{1-R}\right) + \sqrt{\left(\frac{4R}{(1-R)^2} - K^2\right)}. \quad (3)$$

The variation of refractive index versus wavelength are shown in Fig. 4b. Their values at the absorption edge with deposition rates of 0.2, 0.4, 0.6 and 0.8 nm/s are 2.09±0.17, 2.11±0.13, 2.13±0.09 and 2.14±0.15, respectively. The high refractive index for the ZnSe film makes it suitable for use in optoelectronic applications [3]. Furthermore, according to Fig. 4b, the refractive index at shorter wavelengths has a higher value for all samples, which may be associated with the fundamental band gap absorption [25]. It is observed that for all samples, the refractive index has fluctuated with decreasing wavelength, which can be applied in infrared tools [26].

Table 1: The porosity and optical parameters of the ZnSe thin films prepared at different deposition rates

Deposition rate (nm/s)	n (at absorption edge)	Porosity	E_g (eV)
0.2	2.09±0.17	0.52 ±0.17	3.98±0.01
0.4	2.11±0.13	0.73±0.26	3.86±0.01
0.6	2.13±0.09	0.82±0.26	3.76±0.01
0.8	2.14±0.15	0.65±0.28	3.71±0.01

Deposition rate (nm/s)	ε_2 (λ= 550 nm)	ε_1 (λ= 550 nm)	K (λ= 550 nm)
0.2	0.118±0.017	3.91±0.67	0.030±0.002
0.4	0.055±0.007	2.65±0.41	0.017±0.001
0.6	0.029±0.004	2.10±0.42	0.010±0.001
0.8	0.074±0.009	3.16±0.52	0.021±0.001

The refractive index of the films has a direct effect on the porosity of the films. The porosity of the films is obtained by using Eq. (4) [27]:

$$\text{porosity} = \left(1 - \frac{n^2-1}{n_d^2-1}\right). \quad (4)$$

In this equation, n is the refractive index, n_d is the refractive index of pore-free ZnSe where its value is 2.67 [9]. The results of the calculations are presented in Table 1. The porosity of the sample with a deposition rate of 0.6 nm/s is the highest porosity of the films which can show a smaller packing density in this sample. The dielectric constant was calculated in ZnSe thin films according to the following equations:

$$\varepsilon_1 = n^2 - k^2, \quad (5)$$
$$\varepsilon_2 = 2nk. \quad (6)$$

The lower dielectric constant values can lead to induction polarization in material [12]. In the above equations, ε_1 and ε_2 are real and imaginary parts of the dielectric constant, respectively. The variations of the real dielectric constant as a function of wavelength for annealed samples at various deposition rates are shown in Fig. 5. As can be seen, the real dielectric constant with increasing deposition rate up to 0.6 nm/s decreases and thereafter increases.

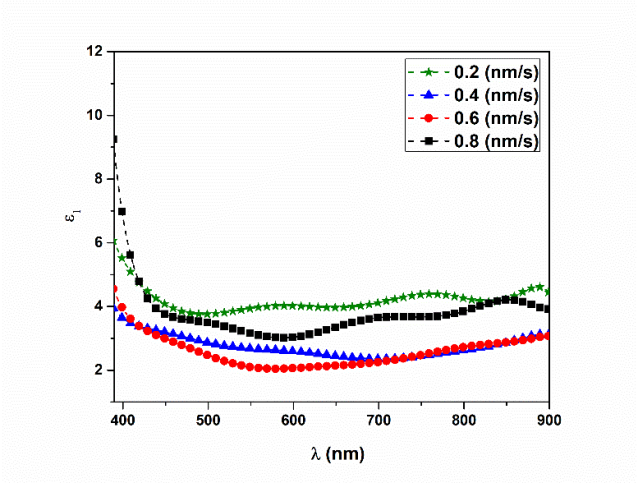

Figure 5. Variation of the real dielectric constant versus the wavelength for samples with different deposition rates.

The values obtained for dielectric constants at 550 nm are shown in Table 1. The real part of the dielectric function reflects the permittivity of the material lattice and the imaginary part is related to the absorption.

In addition, the optical band gap energy was determined based on the derivation of the absorption spectrum fitting (DASF) method. The absorption coefficient ($\alpha(\lambda)$) can be written in terms of λ by the following equation [28]:

$$\alpha(\lambda) = B(hc)^{m-1}\lambda\left(\frac{1}{\lambda}-\frac{1}{\lambda_g}\right)^m, \qquad (7)$$

where λ_g, B, h, c, and m are the wavelengths attributed to the energy gap, a constant, Planck's constant, the velocity of the light, and the optical transition index of charge carrier, respectively. We can substitute $\lambda = \frac{c}{\nu}$ (ν is the light frequency) in Eq. (7) and after some simplifications, we obtain the following equation:

$$\alpha(\lambda)h\nu = B(h\nu - h\nu_g)^m, \qquad (8)$$

and then:

$$\ln(\alpha h\nu) = lnB + m\, ln(h\nu - E_g). \qquad (9)$$

By differentiating both sides of Eq. (9) with respect to $h\nu$ gives:

$$\frac{d\{l\, n(\alpha h\nu)\}}{d(h\nu)} = \frac{m}{(h\nu - E_g)}. \qquad (10)$$

The plot of $\frac{d\{l\, n(\alpha h\nu)\}}{d(h\nu)}$ versus $h\nu$ is shown in Fig. 6. It is clear that this plot has a discontinuity in a certain amount of energy, which is the band gap energy ($h\nu = E_g$). The band gap values of the samples are presented in Table 2. As can be seen, the energy gap decreases from about 3.98±0.01 to 3.71±0.01eV with increasing the deposition rate, which is probably due to the increase of the crystallite size and effect of quantum confinement [29]. The range of optical band gap in our samples is well matched to the optical band gap of ZnSe thin films grown by the chemical bath deposition (CBD) method [30].

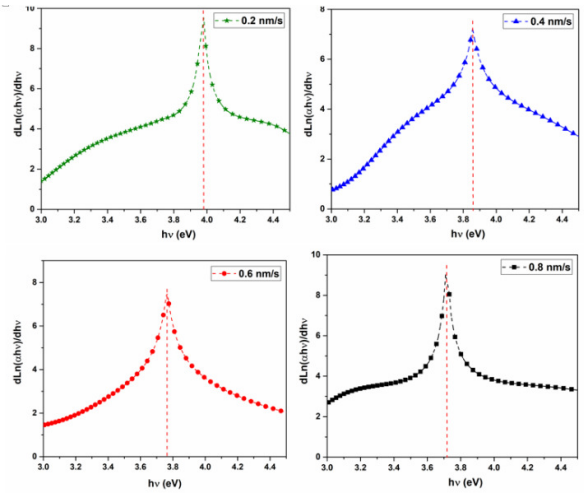

Figure 6. Discontinuity plot of $\frac{d\{l\, n(\alpha h\nu)\}}{d(h\nu)}$ versus $h\nu$ for the ZnSe films deposited at different deposition rates.

The relationship between the refractive index (n) at the absorption edge and the energy band gap of the films can also be investigated according to the Herve–Vandamme model as [31]:

$$n = \sqrt{1 + \left(\frac{13.6}{E_g + 3.47}\right)^2}. \qquad (11)$$

According to this model, n^2 is directly proportional to $(E_g + 3.47)^{-2}$. Fig. 7 shows that the variation of n^2 follows this model well. As can be seen, the refractive index trend at the absorption edge is inversely proportional to the optical band gap trend. Similar behavior is also observed in ZnSe layers fabricated by the chemical bath deposition method (CBD) [30]. It is also well known that the nonlinear optical susceptibility ($\chi^{(3)}$) is inversely related to the energy

band gap and therefore increases with decreasing the energy band gap [32]. According to the literature, materials with higher $\chi^{(3)}$ and lower E_g are suitable options and promising samples in optical device manufacturing and different applications such as fast optical switching devices, optical limiting, and high-speed communication devices [33].

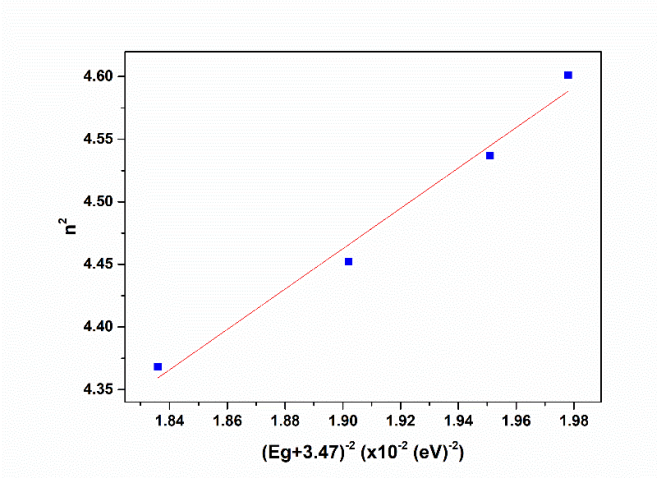

Figure 7. Variations of n^2 as a function of $(E_g + 3.47)^{-2}$.

3.1 Microstructural properties

The structural and microstructural properties of ZnSe thin films, such as the lattice constant, crystallite size, strain, and dislocation density, were also investigated with different deposition rates. In order to specify the mechanisms and determine the structure of these films, the XRD pattern was prepared (see Fig. 8). By studying the XRD analysis of samples, the peaks intensity at the angles of 27.16˚, 45.30˚, and 53.21˚ are related to preferential orientation of the planes (111), (220), and (311), respectively. In addition, by increasing the deposition rate, another peak is created at 72.67˚, which indicates the reflection of the (331) plane. Ion et al. [34] have observed similar peaks for ZnSe films deposited by the Rf-sputtering method. The peaks are in good agreement with JCPDS card No. 37-1463 and the XRD results show that these films crystallize in the cubic structure.

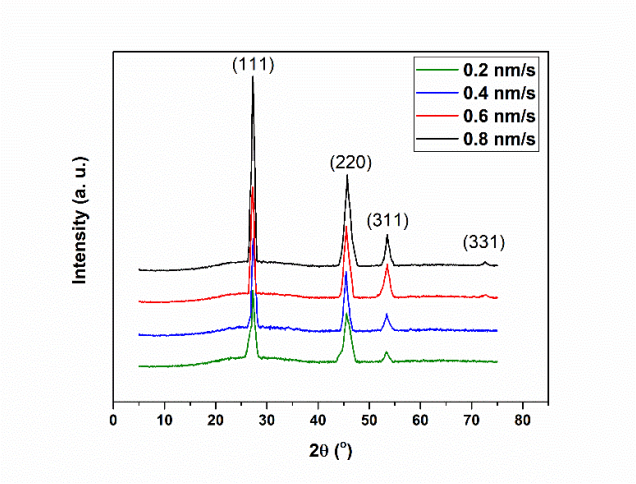

Figure 8. The XRD patterns of the ZnSe samples with different deposition rates.

The crystallite size (D) is also calculated with the help of XRD pattern data using the Williamson-Hall formula from the following equation [35]:

$$\beta \cos\theta = \frac{k\lambda}{D} + 4\varepsilon \sin\theta, \qquad (12)$$

where λ = 1.54056 Å, K is a shape factor which is 0.9 for spherical grains, β is the full width at half maximum (FWHM) in radian, Bragg's diffraction angle (θ) of XRD peak is in degrees, and ε is the strain. The relationship between $\beta \cos\theta$ and $\sin\theta$ for the samples grown at different deposition rates is shown in Fig. 9.

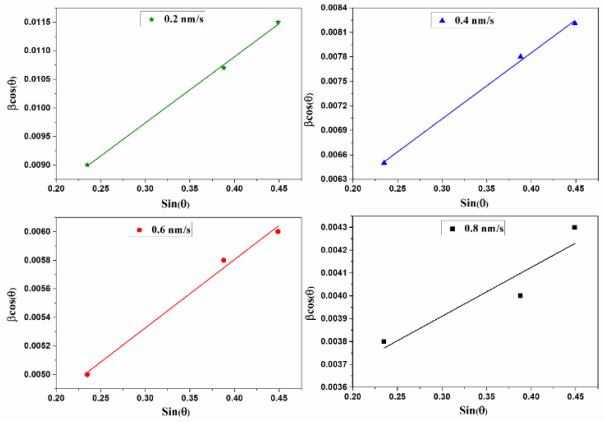

Figure 9. Relationship between $\beta \cos\theta$ and $\sin\theta$ for different samples.

Since a good linear relationship was observed, the strain and crystallite size can be attained from the slope and y-intercept of the linear relationship between

$\beta \cos\theta$ and $\sin\theta$. Also, the lattice constant (a) for the cubic lattice of ZnSe can be obtained from the following equation [30]:

$$a = d\sqrt{h^2 + k^2 + l^2}, \quad (13)$$

where h, k, and l represent the Miller's indexes and d is the lattice spacing. The dislocation density (δ) which is defined as the length of dislocations lines per unit volume of the crystal is calculated from the fallowing relation [36]:

$$\delta = \frac{2\sqrt{3} < \varepsilon^2 >^{\frac{1}{2}}}{b < D >}, \quad (10)$$

where Burgers vector (b) is equal to $\frac{a\sqrt{3}}{2}$. The structural properties of the thin films of ZnSe with four different deposition rates (0.2, 0.4, 0.6, and 0.8nm/s) for the preferential orientation of (111) are given in Table 2.

Table 2: Structural and microstructural properties of ZnSe films with different deposition rates.

Deposition rate (nm/s)	Distance between planes (d) (111) (Å)	Lattice constant (a) (Å)	crystallite size (D) (nm)	Strain (ε) ($\times 10^{-3}$)	Dislocation density (δ) ($\times 10^{-4}$) (nm^{-2})
0.2	3.277±0.063	5.67±0.11	21.6±1.1	2.89±0.04	9.43±0.79
0.4	3.271±0.086	5.66±0.15	28.3±1.4	1.80±0.04	4.49±0.36
0.6	3.265±0.075	5.65±0.13	34.6±1.8	1.14±0.04	2.33±0.25
0.8	3.277±0.092	5.67±0.16	42.9±2.3	0.61±0.02	1.00±0.11

By increasing the deposition rate from 0.2 to 0.6 nm/s, the distance between the planes (111) and the value of the lattice constant decreases and thereafter increases. Among these samples, the sample grown with a deposition rate of 0.6 nm/s is closer to ZnSe bulk lattice constant (5.65 Å). For comparison, the lattice constant values for the samples are in good agreement with the ZnSe thin films grown by the electron beam deposition technique [37].

The dislocation density and strain reduce with the deposition rate. The plot of the dislocation density and the crystallite size versus the deposition rate is shown in Fig. 10. As can be seen, the dislocation density decreases almost linearly by increasing the deposition rate. The crystallite size increases linearly with an increase in the deposition rate.

The results demonstrated that the deposition rate plays an important role in the microstructural properties of ZnSe films, and the crystallinity of the film can be controlled by choosing a suitable deposition rate. A typically SEM image of a ZnSe sample with a thickness of 250 nm and deposition rate of 0.6 nm/s is shown in Fig. 11. According to this image, the average size of grains is about 64 nm (calculated with software), which perfectly confirms the Nano-structure of the sample.

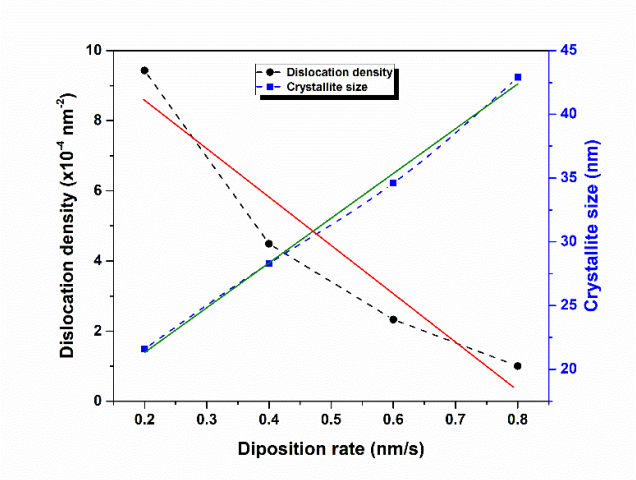

Figure 10. Dislocation density and the crystallite size versus deposition rate.

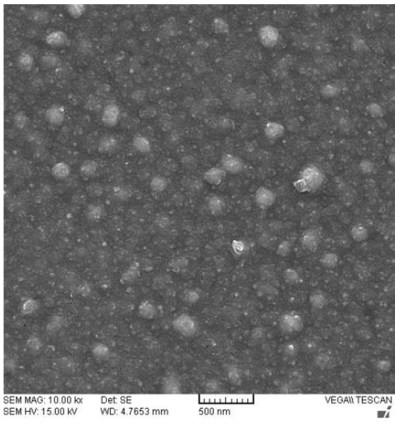

Figure 11. SEM image of the sample with deposition rate of 0.6 nm/s.

4 Conclusions

The ZnSe thin films were deposited on the glass substrate with the thermal evaporation method. The optical parameters of the thin films are generally different from the bulk of the same material. This difference in optical parameters is strongly dependent on the growth conditions of the film. The dependence of the optical and microstructural properties of ZnSe films on the deposition rate was studied and the optical constants of the samples were determined. By increasing the deposition rate between 0.2 and 0.8 nm/s, the refractive index at the absorption edge was changed from 2.09±0.17 to 2.14±0.15. The results showed that the refractive index and band gap energy had an inverse behavior. From the microstructure analysis, it could be concluded that ZnSe films crystallize in a cubic structure, and the dislocation density and crystallite size almost linearly change with the deposition rate. Also, the dislocation density decreased from $(9.43\pm0.79)\times10^{-4}$ to $(1.00\pm0.11)\times10^{-4}$ (nm^{-2}) by increasing the deposition rate. The surface morphology of the films was determined by SEM, which demonstrated the nanostructure of the sample with a deposition rate of 0.6 nm/s. Finally, as a consequence, the deposition rate has a key role in controlling the optical and microstructural properties of ZnSe thin films, and it is necessary for developing a deeper understanding of the performance of devices utilizing these layers.

Acknowledgment

The authors would like to thank the Nanotechnology Research Institute of Shahrekord University for their Laboratory Support.

Conflict of Interest

The authors declare that they have no conflict of interest.

References

[1] L. G. Valluzzi, M. G. Valluzzi, G. N. Darriba, M. Meyer, and L. C. Damonte, “Surfactant and Dopant Addition Effect on Optical and Structural Properties of ZnSe (Te) Nanostructured Semiconductors.” Journal of Alloys and Compounds, **829** (2020) 154488.

[2] M. Imran, A. Saleem, N. A. Khan, A. A. Khurram, and N. Mehmood, “Amorphous to Crystalline Phase Transformation and Band Gap Refinement in ZnSe Thin Films.” Thin Solid Films, **648** (2018) 31.

[3] E. R. Sharaf, I. S. Yahia, M. I. Mohammed, H. Y. Zahran, and E. R. Shaaban, “High Refractive Index and Third-Order Nonlinear Optical Susceptibility of Nanostructured ZnSe/FTO Thin Films: Towards Smart Multifunctional Optoelectronic Materials.” Physica B: Condensed Matter, **602** (2021) 412595.

[4] F. Yao, X. Zhou, and A. Xiong, “Tunable Electronic and Optical Properties of Two-Dimensional ZnSe/AlAs van Der Waals Heterostructure.” Applied Physics A, **126** (2020) 1.

[5] H. H. Yudar, S. Pat, Ş. Korkmaz, S. Özen, and V. Şenay, Zn/ZnSe Thin Films Deposition by RF Magnetron Sputtering, Journal of Materials Science: Materials in Electronics, **28** (2017) 2833.

[6] S. Chuhadiya, R. Sharma, S. L. Patel, S. Chander, M. D. Kannan, and M. S. Dhaka, Thermal Annealing Induced Physical Properties of ZnSe Thin Films for Buffer Layer in Solar Cells, Physica E: Low-Dimensional Systems and Nanostructures, **117** (2020) 113845.

[7] T. D. Lee and A. U. Ebong, A Review of Thin Film Solar Cell Technologies and Challenges, Renewable and Sustainable Energy Reviews **70** (2017) 1286.

[8] H. I. Elsaeedy, A. A. Hassan, H. A. Yakout, and A. Qasem, “The Significant Role of ZnSe Layer Thickness in Optimizing the Performance of ZnSe/CdTe Solar Cell for Optoelectronic Applications.” Optics & Laser Technology, **141** (2021) 107139.

[9] Q. Zhang, H. Li, Y. Ma, and T. Zhai, “ZnSe Nanostructures: Synthesis, Properties and Applications.” Progress in Materials Science, **83** (2016) 472.

[10] S. E. Al Garni and A. F. Qasrawi, "Absorption and Optical Conduction in InSe/ZnSe/InSe Thin Film Transistors." Functional Materials Letters, **9** (2016) 1650019.

[11] S. Ning, G. Feng, H. Zhang, W. Zhang, S. Dai, and S. Zhou, "Fabrication, Structure and Optical Application of Fe2+: ZnSe Nanocrystalline Film." Optical Materials, **89** (2019) 473.

[12] S. Thirumavalavan, K. Mani, and S. Sagadevan, "A Study of Structural, Morphological, Optical and Electrical Properties of Zinc Selenide (ZnSe) Thin Film." Materials Today: Proceedings, **3** (2016) 2305.

[13] F. M. Tezel and İ. A. Kariper, "Effect of PH on the Structural and Optical Properties of Polycrystalline ZnSe Thin Films Produced by CBD Method." International Journal of Modern Physics B, **33** (2019) 1950024.

[14] R. K. Jain, J. Kaur, A. Khanna, and A. K. Chawla, "Tailoring the Structural, Electrical, Optical and Wettability Properties of ZnSe Films by Oblique Angle Thermal Evaporation." Materials Research Express, **6** (2019) 116451.

[15] M. M. Mezdrogina, A. Y. Vinogradov, Y. V Kozhanova, and E. A. Borsuk, "LED Structures Based on ZnO Films Obtained by RF Magnetron Sputtering for the UV Spectral Range." Technical Physics, **65** (2020) 434.

[16] D. V Savin, T. S. Tomilova, S. V Kurashkin, V. B. Ikonnikov, and E. M. Gavrishchuk, "Photoluminescence and Laser Properties of Active Media Based on ZnSe Doped with Cr, Al, Na from Spray Pyrolysis Deposited Films." Laser Physics Letters, **17** (2020) 125802.

[17] D. D. Hile, H. C. Swart, S. V Motloung, R. E. Kroon, K. O. Egbo, and L. F. Koao, "The Effect of Annealing Time on Zinc Selenide Thin Films Deposited by Photo-Assisted Chemical Bath Deposition." Journal of Physics and Chemistry of Solids, **140** (2020) 109381.

[18] Z. Fan, K. Yaddanapudi, R. Bunk, S. Mahajan, and J. M. Woodall, "Interface Studies of Molecular Beam Epitaxy (MBE) Grown ZnSe–GaAs Heterovalent Structures." Journal of Applied Physics, **127** (2020) 245701.

[19] M. R. A. Bhuiyan, M. A. H. Miah, and J. Begum, "Substrate Temperature Effect on the Structural and Optical Properties of ZnSe Thin Films," Journal of Bangladesh Academy of Sciences, **36** (2012) 233.

[20] K. Ou, S. Wang, G. Wan, M. Huang, Y. Zhang, L. Bai, and L. Yi, "A Study of Structural, Morphological and Optical Properties of Nanostructured ZnSe/ZnS Multilayer Thin Films." Journal of Alloys and Compounds, **726** (2017) 707.

[21] Y. Fang, D. Jayasuriya, D. Furniss, Z. Q. Tang, C. Markos, S. Sujecki, A. B. Seddon, and T. M. Benson, "Determining the Refractive Index Dispersion and Thickness of Hot-Pressed Chalcogenide Thin Films from an Improved Swanepoel Method." Optical and Quantum Electronic, **49** (2017) 1.

[22] G. I. Rusu, M. Diciu, C. Pirghie, and E. M. Popa, "Structural Characterization and Optical Properties of ZnSe Thin Films." Applied Surface Science, **253** (2007) 9500.

[23] Z. K. Heiba, A. A. Albassam, and M. B. Mohamed, "Effect of Zn/S Non-Stoichiometric Ratio on the Structural, Optical and Electronic Properties of Nano-ZnS." Applied Physics A, **126** (2020) 1.

[24] A. A. Akl, "Thermal Annealing Effect on the Crystallization and Optical Dispersion of Sprayed V2O5 Thin Films." Journal of Physics and Chemistry of Solids, **71** (2010) 223.

[25] K. V. Saravanan and K. C. J. Raju, "Quasi-Rapid Thermal Annealing Studies on Barium Strontium Titanate Thin Films Deposited on Fused Silica Substrates." Journal of Alloys and Compounds, **571** (2013) 43.

[26] D. Prakash, E. R. Shaaban, M. Shapaan, S. H. Mohamed, A. A. Othman, and K. D. Verma, "Thickness-Dependent Dispersion Parameters, Energy Gap and Nonlinear Refractive Index of

ZnSe Thin Films." Materials Research Bulletin, **80** (2016) 120.

[27] S. B. Khan, Z. Zhang, and S. L. Lee, "Annealing Influence on Optical Performance of HfO2 Thin Films." Journal of Alloys and Compounds, **816** (2020) 152552.

[28] D. Souri and Z. E. Tahan, "A New Method for the Determination of Optical Band Gap and the Nature of Optical Transitions in Semiconductors." Applied Physics B, **119** (2015) 273.

[29] Y. Jiang and N. Bahlawane, "Effect of Nucleation and Growth Kinetics on the Electrical and Optical Properties of Undoped ZnO Films." The Journal of Physical Chemistry C, **114** (2010) 5121.

[30] R. Khalfi, D. Talantikite-Touati, A. Tounsi, and H. Merzouk, "Effect of Deposition Time on Structural and Optical Properties of ZnSe Thin Films Grown by CBD Method." Optical Materials, **106** (2020) 109989.

[31] P. Herve and L. K. J. Vandamme, "General Relation between Refractive Index and Energy Gap in Semiconductors." Infrared Physics & Technology, **35** (1994) 609.

[32] D. Souri, A. R. Khezripour, M. Molaei, and M. Karimipour, "ZnSe and Copper-Doped ZnSe Nanocrystals (NCs): Optical Absorbance and Precise Determination of Energy Band Gap beside Their Exact Optical Transition Type and Urbach Energy." Current Applied Physics, **17** (2017) 41.

[33] S. Ebrahimi, D. Souri, and M. Ghabooli, "Third Order Non-Linear Optical Susceptibility (χ (3)) and Evaluation of Antibacterial Activity of Cu-Doped ZnSe Nanocrystals Fabricated by Hydro-Microwave Technique." Journal of Cluster Science, **30** (2019) 677.

[34] L. Ion, S. Iftimie, A. Radu, V. A. Antohe, O. Toma, and S. Antohe, "Physical Properties Of Rf-Sputtered Znse Thin Films For Photovoltaic Applications: Influence Of Film Thickness." Proceedings of The Romanian Academy Series A-Mathematics Physics Technical Sciences Information Science, **22** (2021) 27.

[35] D. Nath, F. Singh, and R. Das, "X-Ray Diffraction Analysis by Williamson-Hall, Halder-Wagner and Size-Strain Plot Methods of CdSe Nanoparticles-a Comparative Study." Materials Chemistry and Physics, **239** (2020) 122021.

[36] V. Soleimanian and M. Mojtahedi, "A Comparison between Different X-Ray Diffraction Line Broadening Analysis Methods for Nanocrystalline Ball-Milled FCC Powders." Applied Physics A, **119** (2015) 977.

[37] D. N. Papadimitriou, "Vacuum and Liquid-Phase Processing of ZnSe Buffer-Layer for Chalcopyrite Absorber Based Photovoltaic Technology." ECS Journal of Solid State Science and Technology, **7** (2018) 541.